Numerical Calculation of Bubble Growth in Nucleate Boiling From Inception Through Departure

R. C. Lee
Assistant Professor of Mechanical Engineering,
Utah State University,
Logan, UT 84322-4130
Assoc. Mem. ASME

J. E. Nydahl
Professor of Mechanical Engineering,
University of Wyoming,
Laramie, WY 82071
Mem. ASME

The relative contributions of the fundamental mechanisms accounting for the enhanced heat transfer in nucleate boiling are difficult to quantify analytically or experimentally. A comprehensive model was developed that permits some accurate insights into this problem. An essential feature involved the numerical mapping of the complicated geometry to a plane where the bubble and wall boundaries lie along constant coordinate lines. The results show that microlayer evaporation accounts for 87 percent of the enhanced wall heat transfer during saturated boiling of water at 1 atm and 8.5 K wall superheat. In contrast, enhanced convective effects were essentially nonexistent during growth and minimal following departure. The analysis predicts an extremely nonuniform thermal boundary layer around the bubble, and shows that the wall thermal boundary layer regenerates almost immediately following departure.

Introduction

From a microscopic point of view, the two factors accounting for the enhanced heat transfer in nucleate boiling are forced convective effects and latent heat transport. The bubble motion produces enhanced forced convection around the site commonly termed microconvection during growth and liquid-vapor exchange following departure. The latent heat energy required to form the bubble is conducted into the bubble either directly through a liquid microlayer beneath the bubble or indirectly through the bubble cap. Following bubble departure the wall thermal boundary layer near the nucleation site is regenerated by transient conduction.

Early models for the growth of a nucleate boiling bubble (Hsu and Graham, 1961; Van Stralen, 1967; Mikic et al., 1970) neglected the microlayer and modeled the bubble cap heat transfer by assuming a thin, typically uniform, thermal boundary layer. The existence of the microlayer is now an undisputed fact, but the question of its contribution to the enhanced heat transfer in nucleate boiling is not well defined. Depending on the boiling conditions, the estimate of its contribution to the energy required for bubble growth ranges from less than 20 percent to nearly 100 percent (Voutsinos and Judd, 1975; Van Stralen et al., 1975; Judd and Hwang, 1976; Fath and Judd, 1978; Koffman and Plesset, 1983).

Several numerical models of nucleate boiling (Madhaven and Mesler, 1970; Guy and Ledwidge, 1973; Dalle Donne and Ferranti, 1975; Beer et al., 1977; Zijl et al., 1979; Fath, 1981) have been developed, but they incorporated significant simplifications and typically addressed only a portion of the bubble cycle.

Outer Flow Solution

In this paper the axisymmetric Navier-Stokes and energy equations are applied to a nucleate boiling bubble in saturated pool boiling on a horizontal surface, and are solved numerically from inception through departure. The goal was to develop a procedure that can simulate the complete nucleate boiling bubble cycle with a minimum of simplifying assumptions, and thus determine quantitatively and qualitatively the relative importance of the micromechanisms. The bubble geometry during growth and departure is shown in Fig. 1.

Contributed by the Heat Transfer Division and presented at the ASME Winter Annual Meeting, Boston, Massachusetts, December 13-18, 1987. Manuscript received by the Heat Transfer Division November 23, 1987. Keywords: Augmentation and Enhancement, Boiling, Evaporation.

The finite difference formulation uses a numerical grid generation technique that addresses the complicated geometry, time-dependent boundaries,and large grid spacing variation required to resolve both the microlayer and "infinity" boundaries. The technique employed was introduced by Thompson et al. (1974) who took the transformation to be governed by the system of elliptic partial differential equations

$$\alpha r_{\xi\xi} - 2\beta r_{\xi\eta} + \gamma r_{\eta\eta} + J^2(Pr_\xi + Qr_\eta) = 0 \quad (1)$$

$$\alpha z_{\xi\xi} - 2\beta z_{\xi\eta} + \gamma z_{\eta\eta} + J^2(Pz_\xi + Qz_\eta) = 0 \quad (2)$$

where P and Q are arbitrary weighting functions used to control grid spacing. Standard second-order finite difference approximations were used to represent these equations, and the resulting finite difference equations were solved iteratively using Newton-Raphson linearization and successive overrelaxation by lines.

The transformed Navier-Stokes and energy equations for the bulk fluid are

$$(\omega J)_t + (U_c\omega)_\xi + (V_c\omega)_\eta =$$

$$J[(\alpha\omega_{\xi\xi} - 2\beta\omega_{\xi\eta} + \gamma\omega_{\eta\eta})/J^2 + Q'\omega_\eta + P'\omega_\xi - \omega/r^2]/\mathrm{Re} \quad (3)$$

$$(\alpha\psi_{\xi\xi} - 2\beta\psi_{\xi\eta} + \gamma\psi_{\eta\eta})/J^2 + Q''\psi_\eta + P''\psi_\xi - r\omega = 0 \quad (4)$$

$$(TJ)_t + (U_cT)_\xi + (V_cT)_\eta =$$

$$J[(\alpha T_{\xi\xi} - 2\beta T_{\xi\eta} + \gamma T_{\eta\eta})/J^2 + Q'T_\eta + P'T_\xi]/\mathrm{Pe} + uTJ/r \quad (5)$$

where

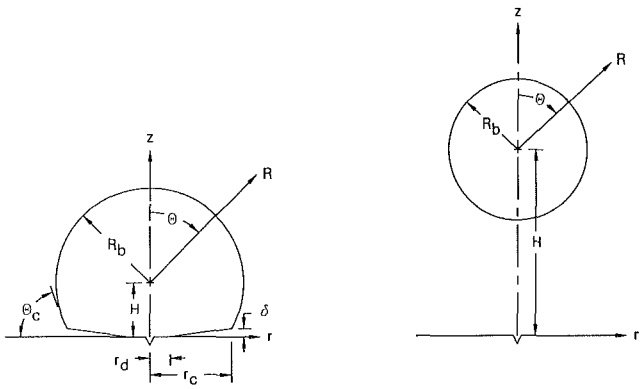

Fig. 1 Bubble geometry during growth and departure

$$P' = P + z_\eta/rJ, \qquad Q' = Q - z_\xi/rJ$$
$$P'' = P - z_\eta/rJ, \qquad Q'' = Q + z_\xi/rJ$$

The finite difference representation of equations (3)–(5) used a fully implicit forward time, central space formulation that was solved, again, using successive overrelaxation by lines.

The vorticity boundary conditions arise from the no-slip velocity condition that was imposed on both the wall and the liquid–vapor interface. A modified form of the technique of Israeli (1970) was employed where the boundary vorticity is iteratively updated according to

$$\omega_{\text{wall}}^{m+1} = \omega_{\text{wall}}^{m} + \Omega |\omega_{\max}/V_0| V_T \tag{6}$$

where Ω is an acceleration parameter, V_0 the stagnation point velocity of the bubble, and V_T the current iteration step tangential velocity. The vorticity along the line of symmetry, the outer boundary, and the dry spot contact point is taken to be zero.

The stream function along the line of symmetry above the bubble is zero, while along the bubble cap

$$\psi = -R_b^2[(H \sin^2\theta)/2 + \dot{R}_b(1-\cos\theta)] \tag{7}$$

The velocity along the microlayer–vapor interface was assumed to be zero, which makes the stream function along the microlayer and bottom wall equal to $\psi(\theta=\pi-\theta_c)$ as found from equation (7). The stream function along the outer boundary is $\psi_{\max}(1-\cos\theta)$ by assuming purely radial flow caused by bubble growth.

The temperature boundary conditions are $T=1$ along the wall, $T=T_g$ along the bubble, and zero temperature gradient along the line of symmetry. The far-field boundary condition is that provided by one-dimensional conduction into a semi-infinite medium.

The initial conditions are, physically, difficult to ascertain and explain much of the uncertainty in experimental measurements at this microscopic level. The initial velocity is taken to be everywhere zero, and the initial temperature field is assumed to be that given by one-dimensional conduction into a semi-infinite medium. The time (t_w^+) before bubble growth begins was determined using the criterion that growth occurs when the fluid temperature at the bubble height from the wall equals the bubble temperature. The resulting transcendental equation is

$$T_{\text{sat}}^+\left(1 + \frac{2\sigma v_{fg,\text{sat}} \sin\theta_c}{r_n^+ h_{fg}}\right) = \text{erfc}\,[r_n^+(1+\cos\theta_c)/2\sin\theta_c(\alpha t_w^+)^{1/2}](T_{\text{wall}}^+ - T_\infty^+) + T_\infty^+ \tag{8}$$

The nucleation cavity radius (r_n^+) chosen for the simulations was the minimum size that would be active.

An extremely important task that must be performed throughout the development of any numerical model is comparison to experimental data, exact solutions, or previous benchmark numerical simulations. Unfortunately, the accurate experimental data associated with nucleate boiling (at the level of a nucleation site) are primarily restricted to measurements of bubble growth rate, where there is considerable scatter. While this comparison was made, an independent measure of the accuracy of the finite difference representation was required. For this reason, numerical experiments were performed based on simpler problems, but with as many of the physical characteristics of the nucleate boiling problem as possible. The three sets of tests that were performed were as follows: (*i*) Stokes' flow motion of a sphere toward a plane wall; comparison to exact solution of Brenner (1961), (*ii*) uniform, steady flow past a stationary sphere at Reynolds numbers from 0.01 to 300, including the isothermal sphere heat transfer problem; comparison to numerous benchmark numerical and experimental data, and (*iii*) impulsively started motion of a sphere in an infinite medium compared to impulsively started flow past a stationary sphere. In all cases the results were within 1 percent of the appropriate comparison solution, thus validating the fundamental accuracy of the computational code. The reader is referred to Lee (1987) for a detailed discussion of these test cases.

Nucleate Boiling Model

The significant assumptions utilized in making a simulation tractable were: (*i*) constant properties, (*ii*) bubble thermodynamic equilibrium, (*iii*) negligible evaporative resistance, (*iv*)

Nomenclature

C_D = drag coefficient = $-F_z/(\pi\rho_l U^{*2} D^{*2}/8)$
C_p = pressure coefficient
D^* = characteristic length = $[\sigma/g(\rho_l - \rho_{g,\text{sat}})]^{1/2}$
g = gravitational acceleration
h = enthalpy
H = distance from wall to center of bubble
J = Jacobian of the transformation = $r_\xi z_\eta - r_\eta z_\xi$
K = liquid thermal conductivity
$\dot{m}$ = mass transfer rate
Nu = Nussselt number = $q'' D^*/K(T_{\text{wall}}^+ - T_{\text{sat}}^+)$
p = pressure
P = transformation weighting function
Pe = Peclet number = Re • Pr
q = heat transfer rate
q'' = heat flux
Q = transformation weighting function; energy
r, z = cylindrical coordinates
R_b = bubble radius
Re = Reynolds number = $U^* D^*/\nu$
t = time
T = temperature = $(T^+ - T_{\text{sat}}^+)/(T_{\text{wall}}^+ - T_{\text{sat}}^+)$
u = radial cylindrical velocity = ψ_z/r
U^* = characteristic velocity = ν/D^*
U_c = contravariant ξ velocity = $r_\eta(z_t - v) + z_\eta(u - r_t)$
v = vertical velocity = $-\psi_r/r$; specific volume
V_c = contravariant η velocity = $r_\xi(v - z_t) + z_\xi(r_t - u)$
$\mathcal{V}$ = volume
α = transformation coefficient = $r_\eta^2 + z_\eta^2$
β = transformation coefficient = $r_\xi r_\eta + z_\xi z_\eta$
γ = transformation coefficient = $r_\xi^2 + z_\xi^2$
δ = microlayer leading edge thickness
η, ξ = transformed coordinates
θ = angular spherical coordinate
θ_c = bubble "contact" angle
ν = kinematic viscosity
ρ = density
σ = surface tension
ψ = stream function
ω = vorticity = $u_z - v_r$
Ω = relaxation parameter

Subscripts

b = bubble value
fg = change in property from liquid to vapor
g = gas value
l = liquid value
ml = microlayer value
sat = value at saturation conditions
wall = value at the wall
∞ = value at infinity

Superscripts

$+$ = dimensional variable

isothermal wall, (*v*) negligible free convection, (*vi*) no-slip velocity boundary condition around the bubble, and (*vii*) specified bubble and microlayer shape.

The energy for bubble growth is found from an integration over the bubble surface of the energy conducted from the bulk fluid

$$\dot{m}h_{fg} = K\int_A T_n^+ dA = q_b \tag{9}$$

with the energy conducted through the dry spot neglected. The volumetric change of the bubble is found through a mass balance

$$(\rho_g \forall_b)_t = \dot{m} \tag{10}$$

The remaining equations necessary to find the bubble radius (R_b^+) as a function of time are the linearized Clasius–Clapeyron equation

$$T_g^+ = T_{\text{sat}}^+ [1 + (p_g - p_{\text{sat}})v_{fg,\text{sat}}/h_{fg,\text{sat}}] \tag{11}$$

and Laplace's equation to determine the pressure increase across the liquid–vapor interface

$$p_g - \bar{p} = 2\sigma/R_b^+ \tag{12}$$

where $\bar{p}$ is the area-averaged external pressure. Equations (9)–(12) and the ideal gas equation of state represent five equations with five unknowns, coupled with the external solution.

Specification of the microlayer geometry shown in Fig. 1 requires the leading edge thickness (δ^+) and the dry spot radius (r_d^+). The leading edge thickness has been characterized both experimentally and theoretically as equal to the hydrodynamic displacement thickness immediately outside of the microlayer, which leads to the relationship

$$\delta^+ = C[\nu t^+]^{1/2} \tag{13}$$

The value of C has been reported to be from 0.3 to 1.3 (Cooper and Lloyd, 1969; Van Ouwerkerk, 1971; Dwyer and Hsu, 1975; Koffman and Plesset, 1983), but values near unity are the most accepted. δ^+ was determined for the simulations using equation (13) with the proportionality constant being parametrically varied.

The dry spot radius was found by assuming that all microlayer mass transfer into the bubble comes entirely from a change of volume of the microlayer

$$q_{ml} = -\dot{m}_{ml}h_{fg} = -h_{fg}\rho_l (\forall_{ml})_t \tag{14}$$

The energy conducted to the liquid–vapor interface is found through the bulk fluid temperature solution and Fourier's law. The quantities of interest are the overall heat transfer through the bubble cap (q_θ) and the microlayer (q_{ml}). In nondimensional form

$$\overline{\text{Nu}}_\theta = \frac{q_\theta}{K(T_{\text{wall}}^+ - T_{\text{sat}}^+)\pi D^*} = 2R_b^2 \int_0^{\pi-\theta_c} \text{Nu}_\theta \sin\theta d\theta \tag{15}$$

and

$$\overline{\text{Nu}}_{ml} = \frac{q_{ml}}{K(T_{\text{wall}}^+ - T_{\text{sat}}^+)\pi D^*} = 2\int_{r_d}^{r_c} \text{Nu}_{ml}\, rdl \tag{16}$$

where l is the coordinate along the microlayer–vapor interface and $\text{Nu}_{ml}(r = r_d)$ is set equal to 0 because it must be nearly that value inside the dry spot.

An important parameter in nucleate boiling is the departure diameter of the bubble determined by a balance of the buoyancy, drag, dry spot excess pressure, and surface tension forces. The approximation of a wedgelike microlayer is adequate for numerical calculation of the heat transfer, but at departure the actual contact angle (ϕ) must be between that shown in Fig. 1 and $\pi/2$, and was taken to be $\pi/4$. The uncertainty in the value of ϕ would be significant except that the dominant forces at departure are the buoyancy and drag forces. The resulting force balance is

$$(\rho_g \forall_b z_{c,t}^+)_t = \forall_b g(\rho_l - \rho_g) - \pi r_d^+ \sigma(2\sin\phi - 1) - \pi\rho_l U^{*2} D^{*2} C_D/8 \tag{17}$$

where z_c^+ is the center of mass of the bubble. Departure occurs when the forces balance to zero, after which the bubble position is found by a numerical integration.

The pressure distribution around the bubble is ascertained from a line integration of the primitive equations. An integration along the line of symmetry from infinity to the bubble stagnation point z_0 gives the stagnation point pressure

$$C_{p,0} = -V_0^2 + \int_{z_0}^{\infty} (4\omega_r/\text{Re} + 2v_t)_{r=0}\, dz \tag{18}$$

where V_0 is the stagnation point velocity. The pressure distribution around the bubble cap can be found most easily by using a spherical coordinate system that moves with the bubble center, resulting in

$$C_p(\theta) = C_{p,0} + 2R_b\{\ddot{H}(1 - \cos\theta) + \int_0^\theta [(\omega_R + \omega/R)/\text{Re} - \dot{R}_b\omega]_{R=R_b} d\theta\} \tag{19}$$

A boundary layer type of assumption that the pressure is only a function of r in the microlayer results in

$$C_p(r) = C_p(\theta = \pi - \theta_c) + 2/\text{Re}\int_{r_c}^{r} \omega_z \text{dr} \tag{20}$$

where $C_p(\theta = \pi - \theta_c)$ is determined from equation (19).

The drag force is determined through an integration of the pressure and viscous forces around the bubble, leaving out the buoyancy and excess pressure forces at the dry spot, which are treated as separate quantities in the force balance (equation (17)). The pressure drag coefficient for the bubble cap is

$$(C_{Dp})_\theta = 4R_b^2 \int_0^{\pi-\theta_c} C_p(\theta)\sin 2\theta d\theta \tag{21}$$

and for the microlayer is

$$(C_{Dp})_{ml} = -8\int_{r_d}^{r_c} C_p(r) r dr \tag{22}$$

where $C_p(\theta)$ and $C_p(r)$ are evaluated using equations (19) and (20), respectively. The friction drag coefficient for the bubble cap is found through an integration of the viscous stress, resulting in

$$(C_{Df})_\theta = 16R_b^2/\text{Re}\left[(1 - \cos 2(\pi - \theta_c))\dot{R}_b/R_b + \int_0^{\pi-\theta_c} \omega\Big|_{R=R_b} \sin^2\theta d\theta\right] \tag{23}$$

The total drag coefficient is then found by summing the above three components ($(C_{Dp})_\theta$, $(C_{Dp})_{ml}$, $(C_{Df})_\theta$).

Results and Discussion

The saturated nucleate boiling situation that was chosen for simulation was water at 1 atm and 8.5 K wall superheat. Water was chosen due to its obvious engineering importance, and the 8.5 K wall superheat makes available the bubble growth data of Staniszewski (1959). The "contact" angle (θ_c) was given a constant value of 60 deg, which provides the best agreement between the bubble shape shown in Fig. 1 and experimental measurements for water (cf. Han and Griffith, 1965).

Two parametric cases were investigated to quantify the impact of the assumed microlayer growth model. One case used the most widely accepted value ($C \sim 1.0$) for the growth constant in equation (13), while the other case used a reasonable lower limit ($C \sim 0.55$).

The computational grid changes dramatically during the course of the simulation, and an indication of the extreme grid spacing variation is provided in Fig. 2. Although the spacing

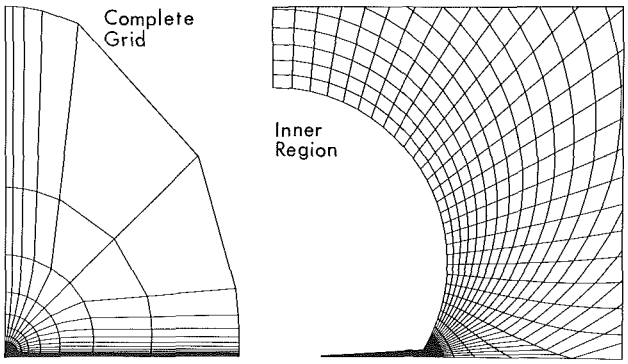

Fig. 2 Computational grid during early growth stage

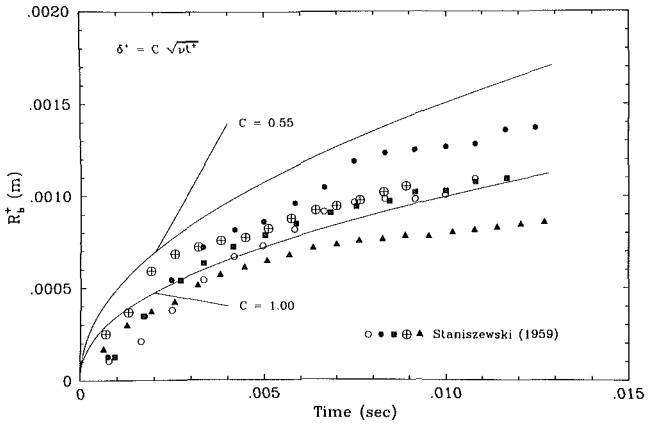

Fig. 3 Bubble growth compared to experimental data

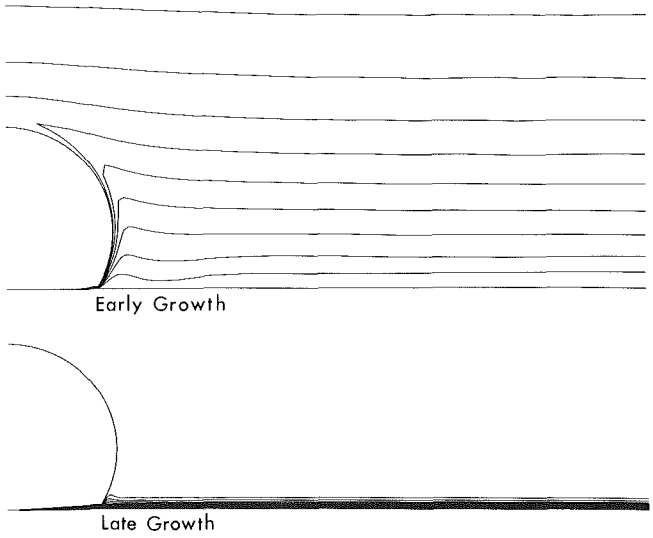

Fig. 4 Isotherms during bubble growth

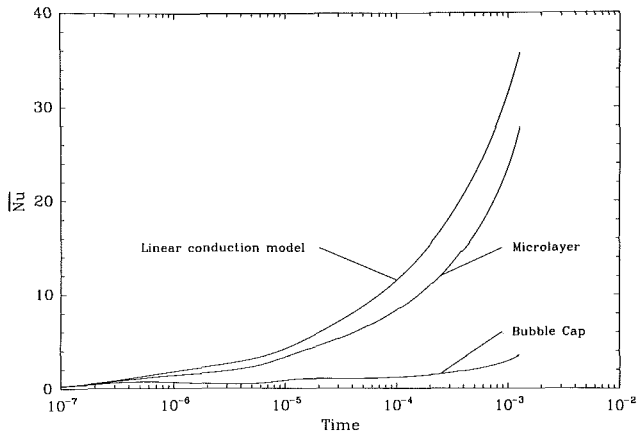

Fig. 5 Average heat transfer rates through the bubble

seems rather coarse near the outer boundary, it is appropriate because the nodes are clustered in regions with large thermal gradients.

The numerical bubble growth rates are compared to the experimental data of Staniszewski (1959) in Fig. 3. There is considerable scatter in the experimental data, although the individual growth curves are well behaved. The best agreement is where the microlayer growth constant was 1.0. For $C = 0.55$, the bubble grows significantly larger, which indicates that the microlayer provides a significant portion of the energy for bubble growth. All numerical results presented from this point are for the base parametric case ($C = 1.0$), unless otherwise indicated.

An indication of the thermal field around the bubble during growth is provided in Fig. 4. Because the bubble represents an isothermal sink in a nonuniform temperature field, the isotherms near the bubble do not uniformly surround the bubble in a boundary-layer-type manner. The folding of isotherms occurs in a thin layer near the bubble and would be very difficult to resolve experimentally, leading, perhaps, to the conclusion drawn by Beer et al. (1977) that the bubble is nonisothermal. For this boiling situation the bubble quickly grows out of the wall thermal boundary layer, with a small portion of the boundary layer wrapping around the cap. During the majority of the growth, however, there is essentially no wrapping of the wall thermal boundary layer around the bubble and the bubble cap heat transfer is essentially restricted to that portion still within the wall boundary layer. This result brings into question those growth models that assume uniform heat transfer around the bubble cap.

The overall energy for bubble growth comes from both the bubble cap and the microlayer, and the average heat transfer from these two regions is shown in Fig. 5. It is evident that the majority of the energy comes from the microlayer; in fact, it contributes nearly 90 percent of the energy for bubble growth for this boiling situation. The dominant importance of microlayer heat transfer explains the impact microlayer thickness has on bubble size. The simplest approach to microlayer heat transfer is to assume one-dimensional steady-state heat conduction and a uniform microlayer thickness of $\delta/2$, which are the assumptions made by Cooper (1969). This leads to the result

$$\overline{Nu}_{ml} \simeq 2(r_c^2 - r_d^2)(1 - T_g)/\delta \qquad (24)$$

which, using simulation values for the variables, is shown along with the numerical results in Fig. 5. The agreement is close enough to warrant the conclusion that microlayer heat capacity is not a significant variable.

Departure proved to be essentially a balance between drag and buoyancy forces, with surface tension forces being an order of magnitude smaller. The departure stage of the ebullition cycle is the most difficult period to simulate accurately because the bubble departs markedly from spherical or truncated spherical shape. The drag calculation during and following departure proved to be very unstable, and the predicted departure diameter of 3.7×10^{-3} m is outside Staniszewski's measured data range of 1.8×10^{-3} to 2.8×10^{-3} m. The ad hoc procedure that was employed during the departure stage was to limit the change in vertical velocity to stabilize the drag calculation, resulting in a slower departure than the force balance called for, but the uncertainty in the shape of the bubble makes more accurate calculation of the vertical velocity su-

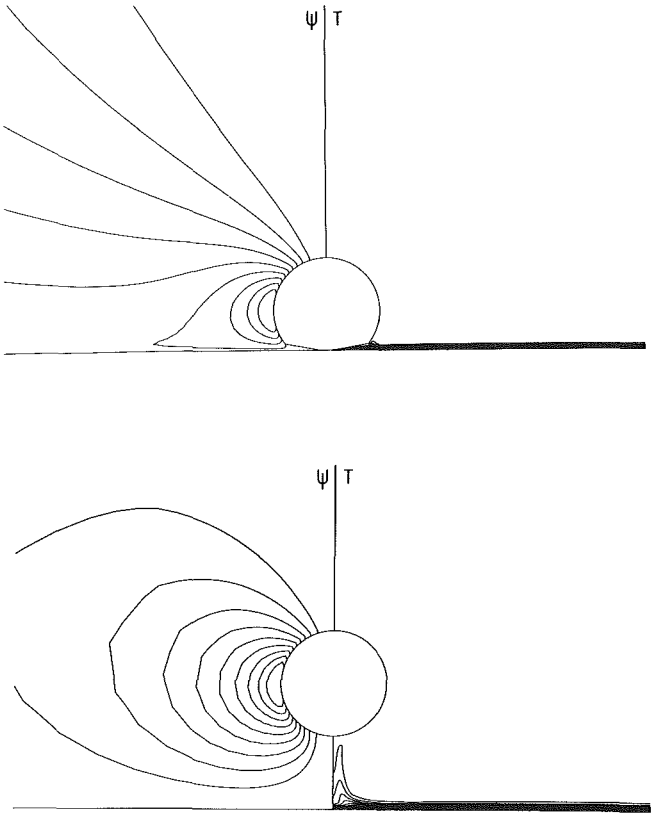

Fig. 6 ψ and T contours during and after departure

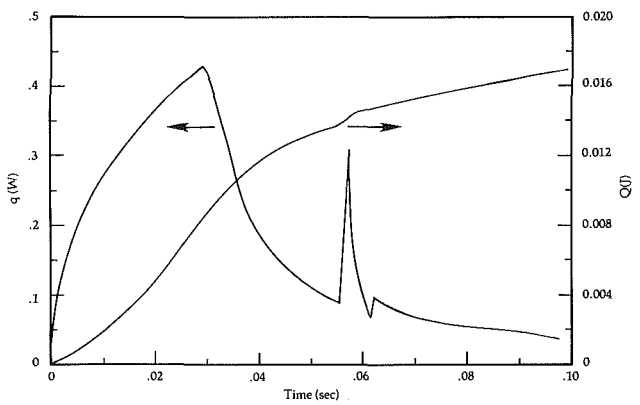

Fig. 7 Excess wall heat transfer and energy

perfluous. The shape of the bubble during departure was modified to satisfy the location of the center of mass by increasing the thickness of the microlayer until the heat transfer in that region became insignificant, and then decreasing the "contact" angle.

The flow and thermal fields during and after departure are shown in Fig. 6. An interesting feature is that the wall scavenging effect caused by departure is limited to the region immediately beneath the bubble, with the maximum effect occurring a small distance from the centerline. The simulation was terminated when the bubble was 2.4 bubble radii from the wall (3.6×10^{-2} s after the bubble had departed) at which time the Reynolds number ($2H^+R_b^+/\nu$) was 1500. An application of the nucleation criteria used to begin the simulation results in a new bubble growing almost immediately following departure when the bubble is only 1.02 bubble radii from the wall. This is not realistic, and results from uncertainty in both the actual nucleation criteria and the numerical results during departure.

Ultimately, the most important value in nucleate boiling is the wall heat transfer. The overall, excess heat transfer rate will be defined as

$$q_{\text{excess}} = 2\pi \int_0^\infty (q'' - q_0'')r^+ dr^+ \tag{25}$$

where q_0'' is the heat transfer that would exist if there were no nucleate boiling. The overall excess energy as a function of time from incipience of growth is defined as

$$Q_{\text{excess}} = \int_0^{t^+} q_{\text{excess}} dt^+ \tag{26}$$

which is a clearer measure of the enhanced heat transfer associated with the nucleate boiling bubble.

The excess heat transfer, along with the overall excess energy, for the simulation is shown in Fig. 7. Due to uncertainties about the point of departure and the subsequent bubble shape and position, the results after the start of departure should be viewed with caution, particularly with respect to the time scales. The first peak in heat transfer is due to the beginning of departure when the microlayer is destroyed, while the second sharp peak in heat transfer is due to the bubble leaving the wall. Although the magnitude of the second peak is probably too large due to numerical uncertainties, its existence is in agreement with experimental temperature measurements beneath a nucleate boiling bubble (cf. Rohsenhow, 1973) that show a small dip in wall temperature at departure. The majority of the energy (87% of the value at the end of the simulation) is provided up to the point of departure, with the remaining energy being due to enhanced convection and transient conduction. Of the energy up to departure, virtually 100 percent is transferred through that portion of the wall comprising the microlayer, pointing to the complete unimportance of microconvection. Keeping in mind that the microlayer provided nearly 90 percent of the energy for bubble growth, it is evident that the microlayer is the dominant mechanism in terms of both bubble growth and the enhanced wall heat transfer.

Concluding Remarks

The major purpose of the numerical simulations was to present a self-consistent formulation that would enable both a qualitative indication of the thermal and fluid fields during bubble growth and departure, and a quantitative comparison of the contributions of the micromechanisms to bubble growth and overall wall heat transfer.

For the conditions simulated, the microlayer proved to be the dominant micromechanism. It provided 90 percent of the energy for bubble growth, and 87 percent of the overall enhanced heat transfer. The enhanced convective heat transfer effects during growth (microconvection) proved to be essentially nonexistent, while the enhanced heat transfer following departure (a combination of enhanced convective effects and transient conduction) provided only 13 percent of the excess heat transfer. There are nucleate boiling problems where microlayer evaporation will not be the dominant mechanism, particularly at high pressures and boiling from small wires. For these cases, the picture of bubble cap heat transfer provided here is of interest. The usual model assumes that the heat transfer is uniform around the bubble cap, but the present results do not support that hypothesis and show that the portion of the bubble cap involved in heat transfer changes significantly during the growth period.

Acknowledgments

The work was performed as part of the Ph.D. dissertation of the first author while at the University of Wyoming.

References

Beer, H., Burow, P., and Best, R., 1977, "Bubble Growth, Bubble Dynamics, and Heat Transfer in Nucleate Boiling, Viewed With a Laser Interferometer," *Heat Transfer in Boiling*, E. Hahne and U. Grigull, eds., Academic Press, New York, pp. 21-52.

Brenner, H., 1961, "The Slow Motion of a Sphere Through a Viscous Fluid Toward a Plane Surface," *Chemical Engineering Science*, Vol. 16, pp. 242-251.

Cooper, M. G., and Lloyd, A. J. P., 1969, "The Microlayer in Nucleate Pool Boiling," *Int. J. Heat Mass Transfer*, Vol. 12, pp. 895-913.

Cooper, M. G., 1969, "The Microlayer and Bubble Growth in Nucleate Pool Boiling," *Int. J. Heat Mass Transfer*, Vol. 12, pp. 915-933.

Dalle Donne, M., and Ferranti, M. P., 1975, "The Growth of Vapor Bubbles in Super-heated Sodium," *Int. J. Heat Mass Transfer*, Vol. 18, pp. 477-493.

Dwyer, O. E., and Hsu, C. J., 1975, "Liquid Microlayer Thickness in Nucleate Boiling on a Heated Surface," *Letters Heat Mass Transfer*, Vol. 2, No. 2, pp. 179-187.

Fath, H. S., and Judd, R. L., 1978, "Influence of System Pressure on Microlayer Evaporation Heat Transfer," ASME JOURNAL OF HEAT TRANSFER, Vol. 100, pp. 49-55.

Fath, H.E.-B.S., 1981, "Microlayer Formation, Evaporation and Bubble Growth in Nucleate Boiling," Ph.D. Dissertation, McMaster University.

Guy, T. B., and Ledwidge, T. J., 1973, "Numerical Approach to Non-spherical Vapour Bubble Dynamics," *Int. J. Heat Mass Transfer*, Vol. 16, pp. 2393-2405.

Han, C. Y., and Griffith, P., 1965, "The Mechanism of Heat Transfer in Nucleate Pool Boiling—Part I. Bubble Initiation, Growth and Departure," *Int. J. Heat Mass Transfer*, Vol. 8, pp. 887-904.

Hsu, Y. Y., and Graham, R. W., 1961, "An Analytical and Experimental Study of the Thermal Boundary Layer and Ebullition Cycle in Nucleate Boiling," NASA TN D-594.

Israeli, M., 1970, "A Fast Implicit Numerical Method for Time Dependent Viscous Flows," *Studies in Applied Math*, Vol. 49.

Judd, R. L., and Hwang, K. S., 1976, "A Comprehensive Model for Nucleate Pool Boiling Heat Transfer Including Microlayer Evaporation," ASME JOURNAL OF HEAT TRANSFER, Vol. C98, pp. 623-629.

Koffman, L. D., and Plesset, M. S., 1983, "Experimental Observations of the Micro-layer in Vapor Bubble Growth on a Heated Surface," ASME *Journal of Heat Transfer*, Vol. 105, pp. 625-632.

Lee, R. C., 1987, "Investigation of the Mechanism of Nucleate Boiling Through Numerical Modelling," Ph.D. Dissertation, University of Wyoming.

Madhaven, S., and Mesler, R., 1970, "A Study of Vapor Bubble Growth on Surfaces," *Heat Transfer 1970*, Vol. 5, Elsevier, Amsterdam.

Mikic, B. B., Rohsenhow, W. M., and Griffith, P., 1970, "On Bubble Growth Rates," *Int. J. Heat Mass Transfer*, Vol. 13, pp. 657-666.

Rohsenow, W. M., 1973, "Boiling," *Handbook of Heat Transfer*, McGraw-Hill, New York.

Staniszewski, B. E., 1959, "Nucleate Boiling Bubble Growth and Departure," M.I.T. DSR Project No. 7-7673, Technical Report No. 16.

Thompson, J. F., Thames, F. C., and Mastin, C. W., 1974, "Automatic Numerical Generation of Body-Fitted Curvilinear Coordinate System for Field Containing Any Number of Two-Dimensional Bodies," *J. Comp. Physics*, Vol. 15, pp. 299-319.

Van Ouwerkerk, H. J., 1971, "The Rapid Growth of a Vapour Bubble at a Liquid-Solid Interface," *Int. J. Heat Mass Transfer*, Vol. 14, pp. 1415-1431.

Van Stralen, S. J. D., 1966, 1967, "The Mechanism of Nucleate Boiling in Pure Liquids and in Binary Mixtures, Parts I-IV," *Int. J. Heat Mass Transfer*, Vol. 9, pp. 995-1020, 1021-1046, Vol. 10, pp. 1469-1484, 1485-1498.

Van Stralen, S. J. D., Sohal, M. S., Cole, R., and Sluyter, W. M., 1975, "Bubble Growth Rates in Pure and Binary Systems: Combined Effect of Relaxation and Evaporation Microlayers," *Int. J. Heat Mass Transfer*, Vol. 18, pp. 453-467.

Voutsinos, C. M., and Judd, R. L., 1975, "Laser Interferometric Investigation of the Microlayer Evaporation Phenomenon," ASME JOURNAL OF HEAT TRANSFER, Vol. 97, No. 1, pp. 88-92.

Zijl, W., Ramakers, F. J. M., and Van Stralen, S. J. D., 1979, "Global Numerical Solutions of Growth and Departure of a Vapour Bubble at a Horizontal Superheated Wall in a Pure Liquid and a Binary Mixture," *Int. J. Heat Mass Transfer*, Vol. 22, pp. 401-420.